KSME

Springer

Journal of Mechanical Science and Technology 38 (9) 2024

Original Article
DOI 10.1007/s12206-024-0841-2

Keywords:
· Parallel manipulator
· Actuation redundancy
· Kinematics performance evaluation
· Optimum design
· Control mode

Correspondence to:
Jun Wu
jhwu@mail.tsinghua.edu.cn

Citation:
Jian, Y., Yu, G., Wu, J., Zhu, B., Tian, Y. (2024). Kinematic performance evaluation method of a 3-DOF redundantly actuated parallel manipulator. Journal of Mechanical Science and Technology 38 (9) (2024) 5075~5085.
http://doi.org/10.1007/s12206-024-0841-2

Received November 16th, 2023
Revised April 26th, 2024
Accepted May 3rd, 2024

† Recommended by Editor Dongho Oh

Kinematic performance evaluation method of a 3-DOF redundantly actuated parallel manipulator

Yunfeng Jian[1,2], Guang Yu[1,2], Jun Wu[1,2], Bin Zhu[1,2] and Yanling Tian[3]

[1]State Key Laboratory of Tribology in Advanced Equipment and Institute of Manufacturing Engineering, Department of Mechanical Engineering, Tsinghua University, Beijing 100084, China, [2]Beijing Key Lab of Precision/Ultra-precision Manufacturing Equipment and Control, Beijing 100084, China, [3]School of Engineering, University of Warwick, Coventry CV4 7AL, UK

Abstract Error transformation can be used to evaluate the kinematic performance of a parallel manipulator. However, the terminal error of redundantly actuated parallel manipulators is difficult to calculate from joint errors. This paper proposes a method to approximate the terminal error of a redundantly actuated parallel manipulator by taking the minimum terminal error among all corresponding nonredundant counterparts. The local Frobenius norm index (LFNI) is proposed to estimate the expectation of terminal error. Additionally, the global Frobenius norm index (GFNI) is introduced to describe the worst case of terminal error in the workspace, which is then used for the optimum design of a RPU-UPR-2UPU redundantly actuated parallel manipulator. After the optimum design, the average root mean square error of the manipulator is reduced. Furthermore, a control mode determination strategy for allocating force/position control to a certain chain is also proposed to minimize the terminal error, whose effectiveness is validated through simulation.

1. Introduction

The parallel mechanism has been widely adopted across various industries, such as aviation simulators, machine tools, and robotics, due to its high stiffness, large loading capacity and low motion inertia [1-3]. However, compared to the traditional series mechanism, the workspace of parallel mechanism is relatively smaller and they are prone to have more singular configurations, which restrict its application scope [4, 5]. To overcome these limitations, the redundant arrangement of actuators has emerged as an effective approach to enlarge the workspace [6, 7], increase stiffness [8] and mitigate singularity issues [9, 10].

However, redundant actuation introduces complex coupling between servo drivers and presents significant challenges for the control of robotic systems. Typically, non-redundant manipulators can use either force control or position control. If all branches of a redundant manipulator are controlled by position mode, considerable internal forces would be introduced due to manufacturing and assembly errors. Hence, to maintain positional accuracy and minimize internal forces, a hybrid force/position control strategy is commonly applied in practice [11-14]. Current researches on mechanisms with actuation redundancy focus on the distribution and coordination of driving forces. Wu et al. optimized force distribution by minimizing key component deformations [15]. Qiu et al. determined the driving torques by reducing the range of actuator torques [16]. Liu et al. proposed a neural network synchronous control method to deal with the actuation coordination problem [17]. Despite these efforts, there remains a gap in the literature regarding the determination of control modes for branch chains in specific configurations, that is, identifying which branches should adopt position control and which should use force control based on performance evaluation.

Kinematic performance evaluation is a fundamental aspect of parallel mechanism design, hinging on the selection of appropriate performance indices. These indices serve as standards

for mechanism performance. Traditionally, two main category of kinematic evaluation indices have been used for parallel manipulators [18]. The first category is based on screw theory and assesses force and energy transfer characteristics. One notable example is the transmission index, which evaluates the efficiency of force transmission [19]. The second category relates closely to the forward Jacobian matrix, focusing on velocity and error transfer characteristics. The most common indexes in this category are the conditioning index [20] and the manipulability index [21]. However, the conditioning index, defined by the ratio of maximum to minimum singular values, merely reflects the relative error instead of the absolute error for a given configuration. Therefore, the conditioning index is unsuitable to be used as a criterion to assess the magnitude of error in different poses of the manipulator [22]. Similarly, the manipulability index, expressed as the product of Jacobian matrix singular values, does not accurately represent the terminal error [22]. Moreover, both indices fail to account for the unique characteristics of redundant mechanisms, such as variations caused by different control modes among different drive branch chains.

In summary, current researches on redundant mechanisms lack significant investigation into the allocation of control modes for branches and the evaluation of kinematic precision particularly considering the unique characteristics of redundant mechanisms. To address these gaps, this paper proposes a novel method for evaluating the kinematic performance of redundantly actuated parallel manipulators through estimating the terminal errors. This method is inspired by the pioneering work of Wu et al. in 2009, who conducted empirical experiments that compare the terminal errors and joint errors of a redundant mechanism with its non-redundant counterpart [23]. They concluded that the error of the end effector in a redundantly actuated parallel manipulator closely resembles that of its non-redundant counterpart.

Building upon this finding, the proposed method investigates the terminal errors of all possible non-redundant counterparts derived from the redundant parallel manipulator. These non-redundant manipulators are created by removing the redundant branch chains while retaining all the constraints on the end effector. By analyzing the minimum among these terminal errors, the terminal error of the redundantly actuated parallel manipulator is approximated.

The contributions include the development of an approximate calculation method for the terminal error of a redundant parallel mechanism. It also involves the establishment of a local performance index LFNI and a global index GFNI for optimum design, as well as the proposal of a novel control strategy for determining the control mode of branch chains in the redundant parallel mechanism.

The rest of the paper is organized as illustrated in Fig. 1. Sec. 2 starts with an introduction to the focus of this study, the redundantly actuated parallel manipulator RPU-UPR-2UPU. In this section, we analyze its degree of freedom (DOF) and establish a comprehensive kinematic model. This is followed by a detailed explanation of the method used to approximate the terminal errors of the redundant mechanism with its non-redundant counterparts. Then two indices are proposed. Secs. 3 and 4 elaborate on their applications in mechanism optimization and control mode determination. Finally, Sec. 5 summarizes the work and offers perspectives for future research.

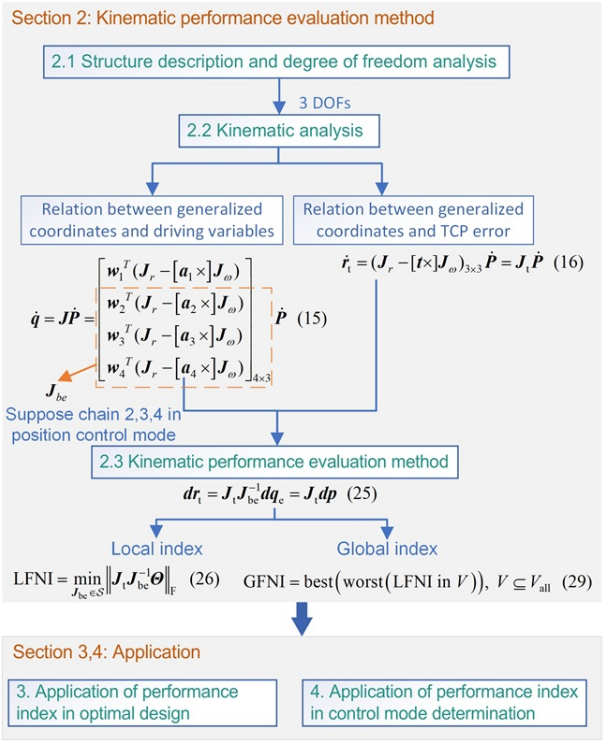

Fig. 1. Structure diagram of the paper.

2. Kinematic performance evaluation method

2.1 Structure description and degree of freedom analysis

A high-stiffness friction stir welding equipment is shown in Fig. 2, featuring a novel RPU-UPR-2UPU parallel manipulator with actuation redundancy. The manipulator is articulated with a combination of universal (U), prismatic (P) and revolute (R) joints. The abbreviation 'RPU' denotes a kinematic chain that connects the base platform to the moving platform through an R joint, followed by a P joint, and then a U joint. The configurations for 'UPR' and 'UPU' adhere to the same logic. The two perpendicular axes of the U joints at the base platform are parallel to each other. The same is true for U joints on the moving platform.

Fig. 3 shows a schematic representation of the parallel manipulator, in which A_i and B_i $(i = 1,2,3,4)$ denote the centers of joints. The base coordinate system $O-XYZ$ is established with its origin O positioned at the midpoint of B_2B_4. The *X*-axis is oriented along B_2B_4, the *Z*-axis is normal to the plane defined by $B_1B_2B_4$, and the *Y*-axis is determined ac-

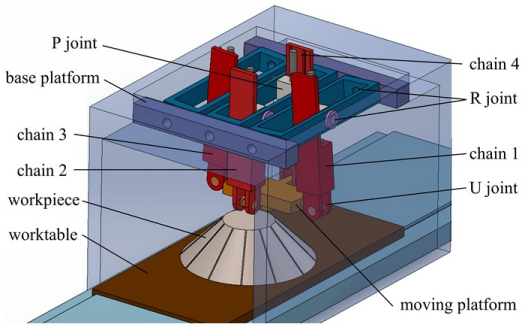

Fig. 2. 3D model of a hybrid equipment for friction stir welding.

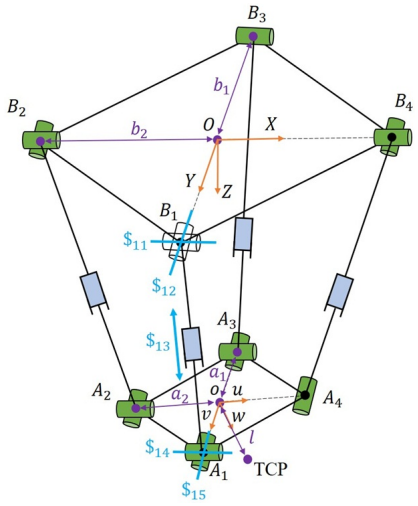

Fig. 3. Twist screws and constraint wrenches of the RPU-UPR-2UPU manipulator.

cording to the right-hand rule. In addition, a body-fixed coordinate system $o-uvw$ is attached to the moving platform, with the origin *o* located centrally on the platform. The axes of the body-fixed coordinate system $o-uvw$ are parallel to the X, Y, and Z axes, respectively.

For convenience, let b_1 be the length of OB_1 and OB_3, and b_2 be the length of OB_2 and OB_4. It is noted that the branch chain A_3B_3 is always on the YOZ plane. Therefore, let the direction vector of branch chains B_1A_1, B_2A_2, B_3A_3 and B_4A_4 be $(0,m_1,n_1)^{\mathrm{T}}$, $(d_2,m_2,n_2)^{\mathrm{T}}$, $(0,m_3,n_3)^{\mathrm{T}}$, $(d_4,m_4,n_4)^{\mathrm{T}}$ and the coordinate of points A_1, A_2, A_3 and A_4 in the base coordinate system $O-XYZ$ be $(0,y_1,z_1)$, (x_2,y_2,z_2), $(0,y_3,z_3)$, (x_4,y_4,z_4). And the direction vector of the *v* axis in the base coordinate system is $(0,f,g)^{\mathrm{T}}$. The twist screw of each joint is shown in Fig. 3.

The twist screws of branch chain A_1B_1 can be expressed as

$$\begin{cases} \$_{11}=(1,0,0,0,0,-b_1)^{\mathrm{T}} \\ \$_{12}=(0,f,g,b_1g,0,0)^{\mathrm{T}} \\ \$_{13}=(0,0,0,m_1,n_1)^{\mathrm{T}} \\ \$_{14}=(1,0,0,z_1,-y_1)^{\mathrm{T}} \\ \$_{15}=(0,f,g,y_1g-z_1f,0,0)^{\mathrm{T}}. \end{cases} \tag{1}$$

By utilizing the reciprocal relationship between twist screws and constraint wrenches, the constraint wrench of chain A_1B_1 can be written as

$$\$_1^{r_1}=(0,0,0,0,-g,f)^{\mathrm{T}}. \tag{2}$$

Following the same analysis process, the constraint wrench system exerted on the moving platform can be obtained as follows:

$$\begin{aligned} \$^r &= \left[\$_1^{r_1} \quad \$_2^{r_1} \quad \$_3^{r_1} \quad \$_3^{r_2} \quad \$_4^{r_1} \quad \$_4^{r_2}\right] \\ &= \begin{bmatrix} 0 & 0 & 0 & 1 & 0 & 0 \\ 0 & 0 & 0 & 0 & 0 & f \\ 0 & 0 & 0 & 0 & 0 & g \\ 0 & 0 & 0 & 0 & 0 & 0 \\ -g & -g & -g & z_3 & -g & -b_2g \\ f & f & f & -y_3 & f & b_2f \end{bmatrix}. \end{aligned} \tag{3}$$

Then, the twist screws of the manipulator can be obtained by solving the reciprocal screw system of Eq. (3)

$$\begin{cases} \$_1=(1,0,0,0,0,0)^{\mathrm{T}} \\ \$_2=(0,f,g,y_3g-z_3f,0,0)^{\mathrm{T}} \\ \$_3=(0,0,0,0,-g,f)^{\mathrm{T}} \end{cases}. \tag{4}$$

In the context of screw theory, the twist screw is defined as $\$=(\boldsymbol{\omega},\boldsymbol{v}_O)$, which is a 6-dimensional vector. Within this representation, $\boldsymbol{\omega}$ represents the angular velocity, and $\boldsymbol{v}_O$ stands for the linear velocity of a point at *O* expressed in the base coordinate system. Therefore, referring to Eq. (4), one can discern that the RPU-UPR-2UPU manipulator possesses a single translational DOF along the *w* axis, complemented by two rotational DOFs, one around the *X* axis and the other about the *v* axis.

2.2 Kinematic analysis

Since the manipulator has 3 DOFs, three generalized variables β, γ, and z are used to describe the pose of the moving platform, where β is the angle of rotation of the moving platform around the X axis, γ is the angle of rotation around the v axis, and z is the distance between O and o. The relationship between the pose of the moving platform and generalized coordinates can be expressed as

$$\mathbf{r}=\mathrm{Rot}(X,\beta)\,\mathrm{Tran}(w,z)=z\begin{bmatrix}0\\-s\beta\\c\beta\end{bmatrix} \tag{5}$$

$$\begin{aligned} \mathbf{R} &= \mathrm{Rot}(X,\beta)\,\mathrm{Rot}(v,\gamma) \\ &= \begin{bmatrix} c\gamma & 0 & s\gamma \\ s\beta s\gamma & c\beta & -s\beta c\gamma \\ -c\beta s\gamma & s\beta & c\beta c\gamma \end{bmatrix} \end{aligned} \tag{6}$$

where s represents the sine function and c represents the cosine function. The relationship between the driving variable $q_i\,(i=1,2,3,4)$ and the generalized coordinates can be established by using the closed-loop constraint equation

$$\mathbf{r}+\mathbf{a}_i=\mathbf{b}_i+q_i\mathbf{w}_i,\quad i=1,2,3,4 \tag{7}$$

where q_i and $\boldsymbol{w}_i$ represent the length and unit direction vector of the branch chain B_iA_i, $\boldsymbol{a}_i$ is the vector of oA_i expressed in the base coordinate system, and $\boldsymbol{b}_i$ is the position vector of joints B_i. Based on Eq. (7), q_i and $\boldsymbol{w}_i$ can be obtained.

$$q_i=\left\|\mathbf{r}+\mathbf{a}_i-\mathbf{b}_i\right\|_2,\quad i=1,2,3,4 \tag{8}$$

$$\mathbf{w}_i=\frac{\mathbf{r}+\mathbf{a}_i-\mathbf{b}_i}{q_i},\quad i=1,2,3,4\,. \tag{9}$$

Taking derivatives on Eqs. (5) and (6) leads to

$$\dot{\mathbf{r}}=\begin{bmatrix}0 & 0 & 0\\ -s\beta & -zc\beta & 0\\ c\beta & -zs\beta & 0\end{bmatrix}\begin{bmatrix}\dot{z}\\ \dot{\beta}\\ \dot{\gamma}\end{bmatrix}=\mathbf{J}_r\dot{\mathbf{P}} \tag{10}$$

$$\begin{aligned}&[\boldsymbol{\omega}\times]=\dot{\mathbf{R}}\mathbf{R}^{-1}\\ &=\begin{bmatrix}0 & 0 & 0\\ 0 & 0 & -1\\ 0 & 1 & 0\end{bmatrix}\dot{\beta}+\begin{bmatrix}0 & -s\beta & c\beta\\ s\beta & 0 & 0\\ -c\beta & 0 & 0\end{bmatrix}\dot{\gamma}\end{aligned} \tag{11}$$

where $[\boldsymbol{\omega}\times]$ represents the skew symmetric matrix of angular velocity. From the correspondence between the skew symmetric matrix and the vector, the following formulation can be obtained

$$\boldsymbol{\omega}=\begin{bmatrix}0 & 1 & 0\\ 0 & 0 & c\beta\\ 0 & 0 & s\beta\end{bmatrix}\begin{bmatrix}\dot{Z}\\ \dot{\beta}\\ \dot{\gamma}\end{bmatrix}=\mathbf{J}_\omega\dot{\mathbf{P}}\,. \tag{12}$$

Taking derivative of Eq. (7), the relationship between terminal velocity and driving variable can be written as

$$\dot{\mathbf{r}}+\boldsymbol{\omega}\times\mathbf{a}_i=\dot{q}_i\mathbf{w}_i+q_i\boldsymbol{\omega}_i\times\mathbf{w}_i \tag{13}$$

where $\boldsymbol{\omega}_i$ denotes the angular velocity of ith branch chain. Applying the dot product with $\boldsymbol{w}_i$ to both sides of Eq. (13) yields

$$\dot{q}_i=\mathbf{w}_i^T(\dot{\mathbf{r}}+\boldsymbol{\omega}\times\mathbf{a}_i)=\mathbf{w}_i^T(\mathbf{J}_r-[\mathbf{a}_i\times]\mathbf{J}_\omega)\dot{\mathbf{P}}\,. \tag{14}$$

Eq. (14) can be rewritten as

$$\dot{\mathbf{q}}=\mathbf{J}\dot{\mathbf{P}} \tag{15}$$

where $\dot{\boldsymbol{q}}=\begin{bmatrix}\dot{q}_1\\ \dot{q}_2\\ \dot{q}_3\\ \dot{q}_4\end{bmatrix}$, $\boldsymbol{J}=\begin{bmatrix}\boldsymbol{w}_1^T(\boldsymbol{J}_r-[\boldsymbol{a}_1\times]\boldsymbol{J}_\omega)\\ \boldsymbol{w}_2^T(\boldsymbol{J}_r-[\boldsymbol{a}_2\times]\boldsymbol{J}_\omega)\\ \boldsymbol{w}_3^T(\boldsymbol{J}_r-[\boldsymbol{a}_3\times]\boldsymbol{J}_\omega)\\ \boldsymbol{w}_4^T(\boldsymbol{J}_r-[\boldsymbol{a}_4\times]\boldsymbol{J}_\omega)\end{bmatrix}_{4\times3}$ is the backward Jacobian matrix of the manipulator. Let l be the tool length and the tool center point (TCP) velocity $\dot{\boldsymbol{r}}_\mathrm{t}$ is

$$\dot{\mathbf{r}}_\mathrm{t}=\dot{\mathbf{r}}+\boldsymbol{\omega}\times\mathbf{t}=(\mathbf{J}_r-[\mathbf{t}\times]\mathbf{J}_\omega)\dot{\mathbf{P}}=\mathbf{J}_\mathrm{t}\dot{\mathbf{P}} \tag{16}$$

where $\mathbf{t}=\mathbf{R}\begin{bmatrix}0 & 0 & l\end{bmatrix}^\mathrm{T}$.

2.3 Performance evaluation index

For a redundantly actuated parallel manipulator with m actuators and n degrees of freedom, its kinematics equation can be expressed as

$$\mathbf{p}=\mathbf{f}(\mathbf{q}),\ \mathbf{q}=\mathbf{f}^{-1}(\mathbf{p}) \tag{17}$$

where $\boldsymbol{p}=[p_1,p_2,\cdots,p_n]^\mathrm{T}$ represents the generalized coordinates of the end effector, $\boldsymbol{q}=[q_1,q_2,\cdots,q_m]^\mathrm{T}$ is the joint displacement. In the case of the RPU-UPR-2UPU manipulator, m = 4 and n = 3. Taking the derivative of Eq. (17) leads to

$$\dot{\mathbf{p}}=\mathbf{J}_\mathrm{f}\dot{\mathbf{q}},\ \dot{\mathbf{q}}=\mathbf{J}_\mathrm{b}\dot{\mathbf{p}} \tag{18}$$

where $\boldsymbol{J}_\mathrm{f}\in\mathbb{R}^{n\times m}$ denotes the forward Jacobian matrix and $\boldsymbol{J}_\mathrm{b}\in\mathbb{R}^{m\times n}$ is the inverse Jacobian matrix. According to the definition of redundantly actuated parallel manipulator, it is easy to get $m>n$, which means $rank(\boldsymbol{J}_\mathrm{b})\le n$. When $rank(\boldsymbol{J}_\mathrm{b})=n$, there are n linearly independent row vectors in $\boldsymbol{J}_\mathrm{b}$ and the redundantly actuated parallel manipulator is in a non-singular configuration.

Let $\mathbf{p}$ and $\boldsymbol{q}$ be any desired configuration in the workspace satisfying $rank(\boldsymbol{J}_\mathrm{b})=n$. Because of the existence of sensor errors, friction, and other factors, the actual configuration deviates from the expected one in the real world and is denoted as $\boldsymbol{p}+\boldsymbol{dp}$ and $\boldsymbol{q}+\boldsymbol{dq}$. When this deviation is relatively small, the error can be approximated by the following linear equation:

$$\mathbf{dq}=\mathbf{J}_\mathrm{b}\mathbf{dp}\,. \tag{19}$$

When the manipulator is in a nonsingular pose, the terminal error can be uniquely determined by n joint errors corresponding to n linearly independent rows in $\boldsymbol{J}_\mathrm{b}$ as expressed in Eq. (20).

$$\mathbf{dp}=\left(\mathbf{J}_\mathrm{be}\right)^{-1}\mathbf{dq}_e \tag{20}$$

where $\boldsymbol{J}_\mathrm{be}\in\mathbb{R}^{n\times n}$ consists of n linearly independent row vectors of $\boldsymbol{J}_\mathrm{b}$ and $\boldsymbol{dq}_\mathrm{e}\in\mathbb{R}^{n\times1}$ is the corresponding error of

driving variables extracted from $\boldsymbol{dq}$. Eq. (20) can be rewritten as

$$(\mathbf{dp})_i = \sum_{j=1}^{n} \left(\mathbf{J}_{\mathrm{be}}^{-1}\right)_{ij} \left(\mathbf{dq}_{\mathrm{e}}\right)_j, \quad i = 1,2,\ldots,n. \tag{21}$$

Let's consider the relation between joint errors to simplify Eq. (21). In general, the relationship between these control input errors is nonlinear rather than linear. And the degree of correlation can be reduced by a control algorithm. Therefore, it can be assumed that the errors of driving variables are linearly independent and have a zero mean. Then the expectation of the sum of squared errors of the end effector can be obtained as follows:

$$\mathrm{E}\left(\left\|\mathbf{dp}\right\|_2^2\right) = \sum_{i=1}^{n}\sum_{j=1}^{n} \left(\mathbf{J}_{\mathrm{be}}^{-1}\right)_{ij}^2 \mathrm{E}\left(\left(\mathbf{dq}_{\mathrm{e}}\right)_j^2\right). \tag{22}$$

Eq. (22) can be written in the matrix form

$$\mathrm{E}\left(\left\|\mathbf{dp}\right\|_2^2\right) = \left\|\mathbf{J}_{be}^{-1}\boldsymbol{\Theta}\right\|_{\mathrm{F}}^2 \mathrm{E}\left(d^2\right) \tag{23}$$

where $\|\cdot\|_{\mathrm{F}}$ denotes the Frobenius norm, $\boldsymbol{\Theta} = \mathrm{diag}\left(\sqrt{\frac{\mathrm{E}((\boldsymbol{dq}_{\mathrm{e}})_1^2)}{\mathrm{E}(d^2)}}, \sqrt{\frac{\mathrm{E}((\boldsymbol{dq}_{\mathrm{e}})_2^2)}{\mathrm{E}(d^2)}}, \cdots, \sqrt{\frac{\mathrm{E}((\boldsymbol{dq}_{\mathrm{e}})_n^2)}{\mathrm{E}(d^2)}}\right)$ and $\mathrm{E}(d^2)$ is the maximum value of $\mathrm{E}((\boldsymbol{dq}_{\mathrm{e}})_i^2)$, $i = 1,2,\cdots,n$. If the errors of the driving variables are independent and identically distributed, then $\mathrm{E}(d^2)$ can be selected as $\mathrm{E}((\boldsymbol{dq}_{\mathrm{e}})_1^2)$ and $\boldsymbol{\Theta}$ will be an identity matrix in this case.

Since $\boldsymbol{J}_{\mathrm{be}}$ consists of n linearly independent row vectors of $\boldsymbol{J}_{\mathrm{b}}$, there are at most C_m^n choices for $\boldsymbol{J}_{\mathrm{be}}$ theoretically. On the other hand, one of the advantages of a redundantly actuated parallel manipulator is less singularity in the workspace; thus, in general, there is at least one choice of $\boldsymbol{J}_{\mathrm{be}}$. Let $\mathcal{S}$ be the set of all the choices of $\boldsymbol{J}_{\mathrm{be}}$. And each choice of $\boldsymbol{J}_{\mathrm{be}}$ that meets the full rank condition corresponds to one particular way of determining the control mode of each actuator, that is, the n branch chains comprising $\boldsymbol{J}_{\mathrm{be}}$ adopt the position control mode, and the rest $m-n$ branch chains adopt the force control mode. This idea leads to the application of the proposed performance evaluation method in control mode determination of redundantly actuated parallel manipulators.

Eq. (23) gives an estimation of the terminal error of a non-redundant parallel manipulator with all constraints of the redundant manipulator virtually applied. Since a redundant manipulator performs better than its corresponding non-redundant one in terms of terminal accuracy, the best performance of all possible non-redundant counterparts is used to estimate the terminal error. Therefore, the local Frobenius norm index (LFNI) can be defined as the estimation of a redundantly actuated parallel manipulator's terminal error under the unit standard deviation of driving variables, i.e., $\mathrm{E}(d^2) = 1$.

$$\mathrm{LFNI} = \min_{\mathbf{J}_{\mathrm{be}} \in \mathcal{S}} \left\|\mathbf{J}_{\mathrm{be}}^{-1}\boldsymbol{\Theta}\right\|_{\mathrm{F}}. \tag{24}$$

If the inhomogeneous problem of the Jacobian matrix is considered, the error of the end effector can be transformed into the position error of tool center point (TCP), which is a very efficient way to measure terminal error, and the Jacobian matrix between joint errors and TCP errors is homogeneous. The error transformation in this situation can be expressed as

$$\mathbf{J}_{\mathrm{t}}\mathbf{J}_{\mathrm{be}}^{-1}\mathbf{dq}_{\mathrm{e}} = \mathbf{J}_{\mathrm{t}}\mathbf{dp} = \mathbf{dr}_{\mathrm{t}} \tag{25}$$

where $\boldsymbol{dr}_{\mathrm{t}}$ represents the TCP error and $\boldsymbol{J}_{\mathrm{t}} \in \mathbb{R}^{n\times n}$ is the transformation matrix between $\boldsymbol{dp}$ and $\boldsymbol{dr}_{\mathrm{t}}$. In this case, LFNI can be expressed as

$$\mathrm{LFNI} = \min_{\mathbf{J}_{\mathrm{be}} \in \mathcal{S}} \left\|\mathbf{J}_{\mathrm{t}}\mathbf{J}_{\mathrm{be}}^{-1}\boldsymbol{\Theta}\right\|_{\mathrm{F}}. \tag{26}$$

In order to assess the performance across the whole workspace, two possible global comprehensive indexes are presented. One is taking the average of the local index in the workspace:

$$\bar{\eta} = \frac{\int \eta dV}{V} \tag{27}$$

where η is the local index, $\bar{\eta}$ is the global index and V is the workspace. The other is the worst-best subsampling method, which is similar to a two-layer convolutional neural network (CNN). In the first layer, the workspace acts as the convolution kernel over the reachable workspace, and the max pooling method is applied. And in the second layer, the convolution kernel is the whole feature map, and another pooling method is used. This process is shown in Fig. 4. The number in each square corresponds to the local index associated with a certain pose. The smaller the local index is, the better the manipulator performs. Thus, using the worst-best subsampling method, the global comprehensive index can be expressed as

$$\bar{\eta} = \mathrm{best}\left(\mathrm{worst}\left(\eta \text{ in } V\right)\right),\ V \subseteq V_{\mathrm{all}} \tag{28}$$

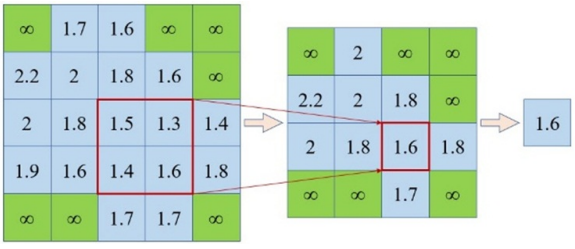

Fig. 4. The worst-best subsampling method (∞ means the configuration is unreachable for the manipulator).

where V_{all} represents the reachable space.

From the worst-best subsampling process, one may see that the global comprehensive index represents the worst case in the best workspace. If the reachable workspace is too small, the global comprehensive index might be infinite. So the worst-best subsampling method considers both the size of the workspace and the worst case within the workspace. It is more reasonable to adopt it for a comprehensive evaluation of the terminal error in the workspace. Therefore, the global Frobenius norm index (GFNI) is defined as

$$\text{GFNI} = \text{best}\left(\text{worst}\left(\text{LFNI in } V\right)\right),\ V \subseteq V_{\text{all}}. \tag{29}$$

When a certain control scheme is used, $\mathrm{E}(d^2)$ will be bound in the workspace. At this point, if GFNI decreases, it is reasonable to believe that the terminal error will also decrease.

3. Application of performance index in optimal design of the RPU-UPR-2UPU manipulator

3.1 Optimal design based on GFNI

In order to ensure consistent requirements for driving motors, the manipulator is intentionally designed to be symmetric, that is, $|\boldsymbol{a}_1| = |\boldsymbol{a}_3|$, $|\boldsymbol{a}_2| = |\boldsymbol{a}_4|$, $|\boldsymbol{b}_1| = |\boldsymbol{b}_3|$, and $|\boldsymbol{b}_2| = |\boldsymbol{b}_4|$. As $|\boldsymbol{a}_1|$, $|\boldsymbol{a}_2|$, $|\boldsymbol{b}_1|$, and $|\boldsymbol{b}_2|$ are the key parameters to represent the shape of the base and the moving platform, they are chosen to be the optimization variables. Since the workspace grows with the increase in initial limb length l_0, it is necessary to eliminate the effect of l_0 on the size of the workspace. Therefore, l_0 is selected as a dimensional factor, and the optimization problem can be expressed as

$$\begin{aligned} &\min \text{GFNI}(\boldsymbol{\lambda}) \\ &s.t.\ 0.1 \prec \boldsymbol{\lambda} \prec 1.5\lambda_0 \end{aligned} \tag{30}$$

where $\boldsymbol{\lambda} = [\lambda_1, \lambda_2, \lambda_3, \lambda_4] = \left[\frac{|\boldsymbol{a}_1|}{l_0}, \frac{|\boldsymbol{a}_2|}{l_0}, \frac{|\boldsymbol{b}_1|}{l_0}, \frac{|\boldsymbol{b}_2|}{l_0}\right]$. Other parameters hidden in the optimization are set to

$$\begin{aligned} &V_{\text{work}}: \Delta(z) = 0.1\text{m},\ \Delta(\beta) = 0.1\text{rad},\ \Delta(\gamma) = 0.1\text{rad} \\ &l_0 = 0.5\text{m},\ l = 0.2\text{m},\ \boldsymbol{\Theta} = \mathbf{I}_3,\ \Delta = 0.05 \end{aligned} \tag{31}$$

where Δ represents the sampling step. The optimization problem is solved by using MATLAB's fmincon function. The initial solution $\boldsymbol{\lambda}_0$ is set to match the parameters in Ref. [16], specifically $\boldsymbol{\lambda}_0 = [0.6, 0.4, 1.2, 0.7]$. The subsequent results are as follows:

$$\begin{aligned} &\boldsymbol{\lambda}^* = [0.90 \quad 0.60 \quad 1.54 \quad 0.40] \\ &V_{\text{work}}^*: z \in [0.55\text{m}, 0.65\text{m}],\ \beta \in [-0.05\text{rad}, 0.05\text{rad}], \\ &\qquad \gamma \in [-0.2\text{rad}, -0.1\text{rad}],\ \text{GFNI} = 1.4103 \end{aligned} \tag{32}$$

Table 1. Geometrical parameters of the manipulator.

Parameter	Before optimization	After optimization	Unit
$\|\boldsymbol{a}_1\| = \|\boldsymbol{a}_3\|$	0.3	0.45	m
$\|\boldsymbol{a}_2\| = \|\boldsymbol{a}_4\|$	0.2	0.30	m
$\|\boldsymbol{b}_1\| = \|\boldsymbol{b}_3\|$	0.6	0.77	m
$\|\boldsymbol{b}_2\| = \|\boldsymbol{b}_4\|$	0.35	0.20	m
l_0	0.5	0.5	m

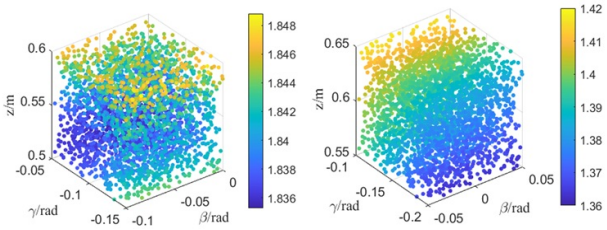

(a) Before optimization (b) After optimization

Fig. 5. Distribution of LFNI in workspace.

Table 1 summarizes the geometrical parameters of the manipulator before and after the optimization.

3.2 TCP error distribution in the workspace

For convenience, let manipulators A and B represent the manipulator before optimization and after optimization, respectively. The GFNI of the manipulator A is 1.847, and its optimal workspace is $z \in$ [0.5 m, 0.6 m], $\beta \in$ [-0.1 rad, 0 rad] and $\gamma \in$ [-0.15 rad, -0.05 rad]. The distribution of LFNI for manipulators A and B in the workspace is shown in Fig. 5. It can be concluded that LFNI in manipulator B is smaller than in manipulator A, as expected in the optimization process.

To validate the effectiveness of the optimization process, the TCP errors of manipulators A and B are simulated under the same joint errors. Wang et al. [24] discovered that errors of branch chains in position control mode were limited to ± 0.1 mm during a force/position hybrid control experiment conducted on a comparable-sized redundantly actuated parallel manipulator. Therefore, in the simulation, errors of the branch chains in position control mode are generated uniformly and randomly within the range of [-0.1 mm, 0.1 mm]. The simulation algorithm for TCP error is shown in Algorithm 1.

In the simulation, 10000 configurations are randomly selected in the workspace, with each pose simulated 100 times. The tool length is set to 0.2 m. All settings in the simulation are summarized in Table 2. After simulation, an array $\boldsymbol{P}_e$ is obtained, whose size is 10000×3×100. Calculating root mean square (rms) error for each pose using the 100-simulation data for that pose, the TCP error is obtained in a statistical sense. The distribution of TCP error along the x, y, and z direction within the workspace are depicted in Figs. 6(a)-(c) respectively by the form of histogram. The distribution of TCP error length within the workspace is shown in Fig. 6(d). Table 3 summa-

Algorithm 1. Simulate TCP errors in whole workspace.

Input: N_c : configuration number; N_t : error generation times; $\boldsymbol{P}$: configurations selected
Output: $\boldsymbol{P}_e$: TCP errors;
1: set $i \leftarrow 0$
2: while $i < N_c$ do
3: set $j \leftarrow 0$
4: while $j < N_t$ do
5: $\boldsymbol{p} \leftarrow \boldsymbol{P}(i)$
6: $\boldsymbol{q} \leftarrow backward\_kinematics(\boldsymbol{p})$
7: $\boldsymbol{q}_r(h) \leftarrow \boldsymbol{q}(h) + rand(-0.1mm, 0.1mm)$, $h = 2,3,4$
8: $\boldsymbol{p}_r \leftarrow forward\_kinematics(\boldsymbol{q}_r(2), \boldsymbol{q}_r(3), \boldsymbol{q}_r(4))$
9: $\boldsymbol{P}_e(i,j) \leftarrow \boldsymbol{p} - \boldsymbol{p}_r$
10: $j \leftarrow j+1$
11: $i \leftarrow i+1$

Table 2. Settings for simulating TCP errors in whole workspace.

Parameter	Value
Error of chain 2	[-0.1 mm, 0.1 mm]
Error of chain 3	[-0.1 mm, 0.1 mm]
Error of chain 4	[-0.1 mm, 0.1 mm]
Number of configurations	10000
Number of simulation times	100

Table 3. TCP error in the workspace.

	Manipulator A		Manipulator B	
	Range (μm)	Mean (μm)	Range (μm)	Mean (μm)
x direction	0-102	34.94	0-66	22.68
y direction	0-284	82.49	0-231	67.29
z direction	0-131	37.33	0-112	33.71
Length	6-313	106.98	4-257	86.56

rizes the distribution range and mean of TCP error.

From Table 3, manipulator B exhibits a significant reduction in mean TCP error to manipulator A in all directions. The mean TCP error along the x direction sees the most substantial decrease, with a reduction of approximately 35.1 %. The mean TCP error along the y and z direction also decrease, with reductions of 18.4 % and 9.7 %, respectively. Additionally, the mean TCP error length decreases by 19.1 %.

The maximum TCP error is also reduced for manipulator B. The maximum TCP error along the x direction is reduced to 66 μm, a decrease of 35.3 %. The maximum TCP error along the y and z directions decreases to 231 μm and 112 μm, respectively, representing reductions of 18.7 % and 14.5 %. The maximum TCP error length decreases to 257 μm, a reduction of 17.9 %.

These results demonstrate the effectiveness of the optimization process in reducing the TCP error, as indicated by the decrease in the GFNI index.

Table 4. The root mean square error of the TCP of manipulators A and B.

Manipulator A	Manipulator B
$\sqrt{\frac{1}{N}\sum e_x^2}$ = 41.96 μm	$\sqrt{\frac{1}{N}\sum e_x^2}$ = 27.2 μm
$\sqrt{\frac{1}{N}\sum e_y^2}$ = 98.3 μm	$\sqrt{\frac{1}{N}\sum e_y^2}$ = 80.3 μm
$\sqrt{\frac{1}{N}\sum e_z^2}$ = 46.2 μm	$\sqrt{\frac{1}{N}\sum e_z^2}$ = 42.1 μm

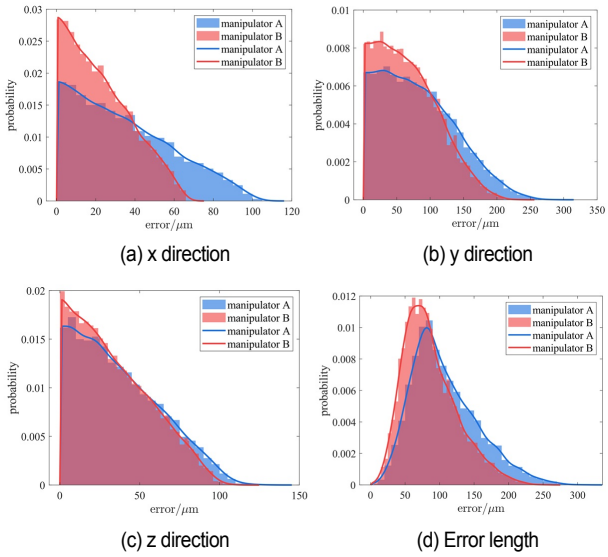

(a) x direction (b) y direction

(c) z direction (d) Error length

Fig. 6. Distribution of TCP error in the workspace.

3.3 Tracking error of the manipulator before and after optimization

To verify the optimization process of the manipulator further, manipulators A and B, with chain 1 being force control mode, move along a typical trajectory as expressed in Eq. (33). Here chain 1 represents branch chain A_1B_1 and chain 2, chain 3, and chain 4 follow the same logic.

$$\begin{cases} z = z_{min} + 0.025t \\ \beta = \frac{1}{2}(\beta_{min} + \beta_{max}) + 0.05\sin \pi t \\ \gamma = \frac{1}{2}(\gamma_{min} + \gamma_{max}) + 0.05\cos \pi t \\ t \in [0,4] \end{cases} \tag{33}$$

where $z_{\min}$ is the minimum value of z in the workspace; $\beta_{\min}$ and $\beta_{\max}$ represent the minimum and maximum value of β in the workspace; and $\gamma_{\min}$ and $\gamma_{\max}$ denote the minimum and maximum value of γ in the workspace. The tracking error simulation algorithm is as follows:

After simulation, their tracking errors are compared, as shown in Figs. 7, 8, and Table 4. In Fig. 7, the trajectory centers have been shifted to the origin for easier comparison.

Algorithm 2. Simulate tracking errors with chain 1 in force control and others in position control.

Input: $\boldsymbol{P}$: configurations in the trajectory
Output: $\boldsymbol{P}_e$: errors of the end effector along trajectory
1: set $i \leftarrow 0$, $N \leftarrow \text{size}(\boldsymbol{P})$
2: while $i < N$ do
3: $\boldsymbol{q} \leftarrow backward\_kinematics(\boldsymbol{P}(i))$
4: for $h \leftarrow 2$ to 3 do
5: $\boldsymbol{q}_r(h) \leftarrow \boldsymbol{q}(h) + rand(-0.1mm, 0.1mm)$
6: $\boldsymbol{p}_r \leftarrow forward\_kinematics(\boldsymbol{q}_r)$
7: $\boldsymbol{P}_e(i) \leftarrow \boldsymbol{P}(i) - \boldsymbol{p}_r$
8: $i \leftarrow i+1$

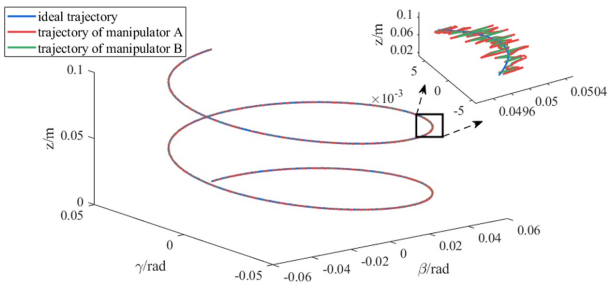

Fig. 7. Trajectory of manipulators A and B, whose centers are shifted to the origin.

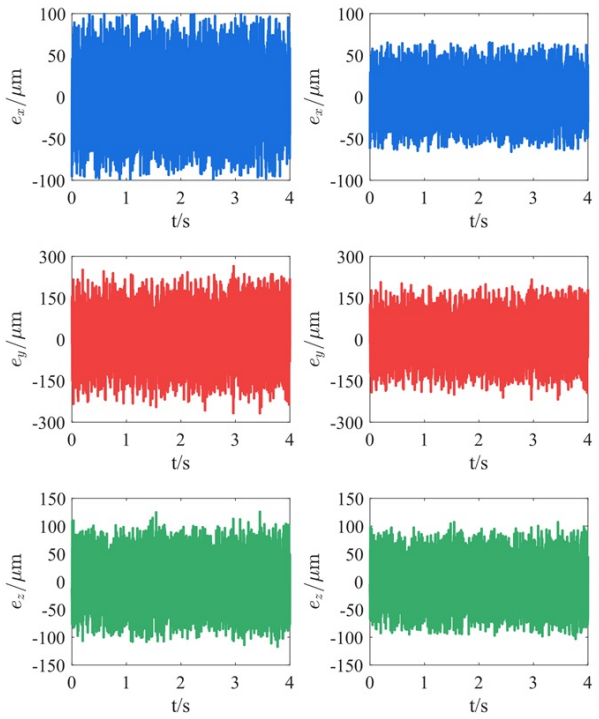

(a) Before optimization (b) After optimization

Fig. 8. TCP error along the *x*, *y*, and *z* directions.

It can be observed that the TCP tracking error of the optimized manipulator is smaller in the X , Y , and Z directions compared to the original one. Specifically, the error in the X direction is significantly reduced by approximately 35.1 %, whereas the errors in the Y and Z directions are reduced by 18.3 % and 8.97 %, respectively. It also shows that the optimum design of the redundantly actuated parallel manipulator based on GFNI is effective.

4. Application of performance index in control mode determination

4.1 Control mode determination strategy

In general, some chains are controlled by position mode, while others are controlled by force mode for a redundantly actuated parallel manipulator. In position control mode, the primary objective is to achieve the desired position of the end effector. The purpose of force control mode is to ensure the distribution of the driving forces to prevent harm caused by an unexpected rush [25]. Theoretically, any chain can be selected to adopt the force control mode, while others adopt the position control mode. However, different control modes affect the manipulator's performance. Based on Eq. (23), the terminal error of the redundantly actuated parallel manipulator can be estimated by considering the joint errors of the chains operating in position control mode. For the same error distribution of joint errors, the terminal error will also be different due to different choices of control mode. Therefore, in order to reduce the terminal error, LFNI is used to determine the chain candidate for force control mode. For convenience, let $E(h)$ represent the estimation of the magnitude of the terminal error with branch chain h in force control mode under the unit standard deviation of driving variables. Based on Eq. (23), $E(h)$ can be expressed as

$$E(h) = \left\| \mathbf{J}_t \mathbf{J}_{be}^{-1} \boldsymbol{\Theta} \right\|_F = \left\| \mathbf{J}_t \left(\left(\mathbf{J}_b \right)_{ij, i \neq h} \right)^{-1} \boldsymbol{\Theta} \right\|_F . \tag{34}$$

According to the analysis in Sec. 2.3, LFNI represents the minimum terminal error in a given configuration. Thus if $E(h)$ equals LFNI in certain poses in the workspace, force control mode should be applied to chain h, while position control mode should be applied to the remaining chains. To be more specific, let branch chain k be the chain in force control mode in a real application. It should satisfy

$$k \in \mathcal{S}_c = \left\{ h \,\middle|\, \exists \mathbf{p} \in V_{\text{work}}, E(h) = \text{LFNI} = \min_{\mathbf{J}_{be} \in \mathcal{S}} \left\| \mathbf{J}_t \mathbf{J}_{be}^{-1} \boldsymbol{\Theta} \right\|_F \right\} . \tag{35}$$

If several branch chains are contained in the choice set $\mathcal{S}_c$, the chain that appears most frequently is recommended. When the position/force switching control is permitted, force control mode should be applied on the chain that makes $E(h)$ locally reach LFNI.

When one particular direction of the terminal error is concerned, a little modification should be made to the control

Table 5. The average root mean square error of TCP along the trajectory of manipulator B.

Chain in force control mode	E(rms(e_x))	E(rms(e_y))	E(rms(e_z))	E(rms($\|e\|$))
Chain 1	**27.5**	80.2	41.6	86.01
Chain 2	50.8	**47.9**	51.5	81.59
Chain 3	**27.5**	80.1	41.5	85.98
Chain 4	48.5	**47.9**	42.2	**76.29**
$\arg\min_{h=1,2,3,4} E(h)$	48.5	**47.9**	42.2	**76.29**
$\arg\min_{h=1,2,3,4} EX(h)$	**27.5**	80.2	41.6	86.01
$\arg\min_{h=1,2,3,4} EY(h)$	48.5	**47.9**	42.3	**76.29**
$\arg\min_{h=1,2,3,4} EZ(h)$	29.8	77.7	**40.2**	84.47

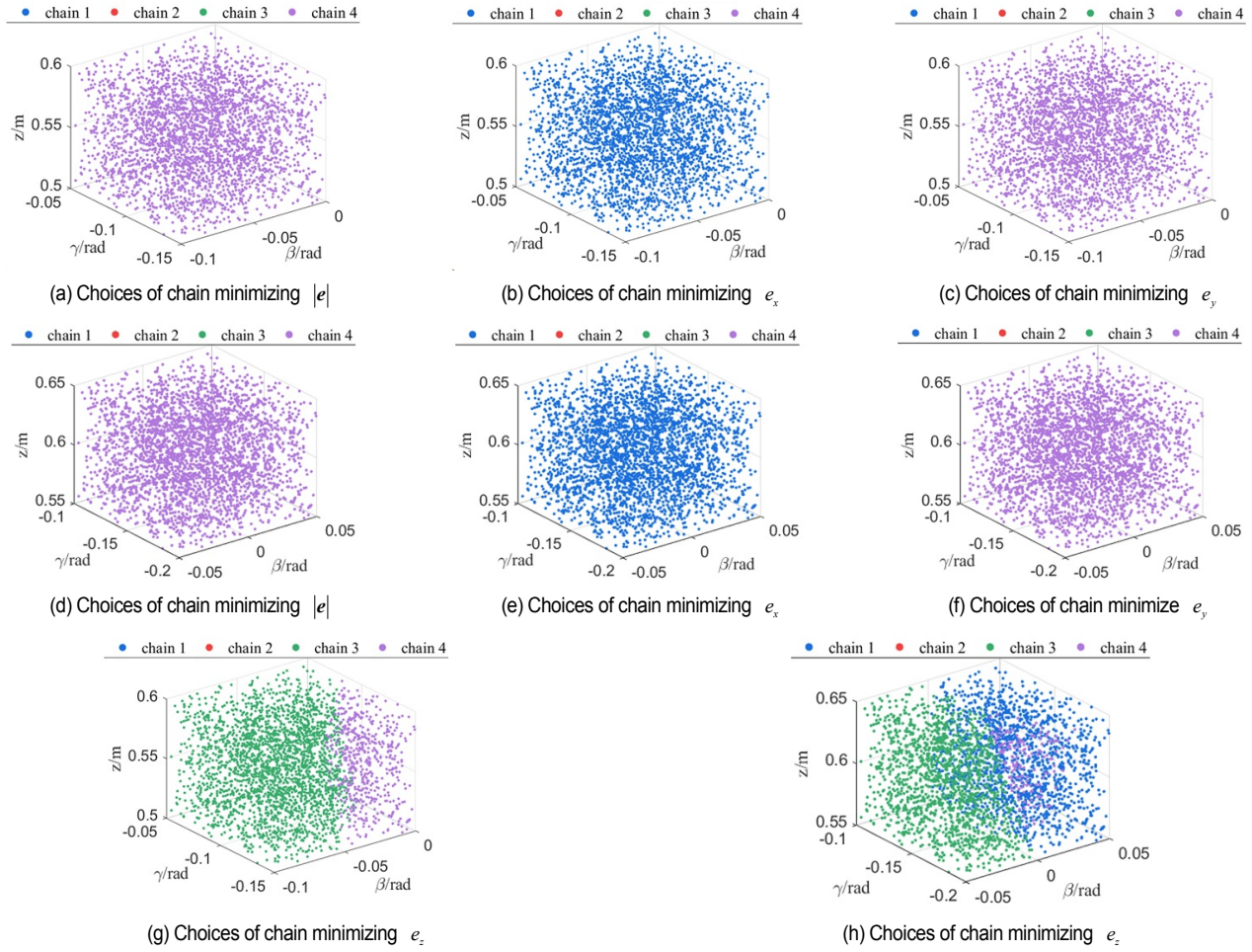

(a) Choices of chain minimizing $|e|$ (b) Choices of chain minimizing e_x (c) Choices of chain minimizing e_y

(d) Choices of chain minimizing $|e|$ (e) Choices of chain minimizing e_x (f) Choices of chain minimize e_y

(g) Choices of chain minimizing e_z (h) Choices of chain minimizing e_z

Fig. 9. Distribution of chain choices in force control mode: (a), (b), (c), (g) before optimization; (d), (e), (f), (h) after optimization.

mode determination strategy. For instance, if the terminal error of X direction is concerned, the chain that makes $EX(h)=\left\|\mathbf{\Lambda}_x\mathbf{J}_t\mathbf{J}_{be}^{-1}\mathbf{\Theta}\right\|_F$ locally get its minimum value is selected to apply force control, where $\mathbf{\Lambda}_x=\mathrm{diag}(1,0,0)$. Similarly, for Y and Z directions, the criterion would be $EY(h)=\left\|\mathbf{\Lambda}_y\mathbf{J}_t\mathbf{J}_{be}^{-1}\mathbf{\Theta}\right\|_F$ and $EZ(h)=\left\|\mathbf{\Lambda}_z\mathbf{J}_t\mathbf{J}_{be}^{-1}\mathbf{\Theta}\right\|_F$ respectively, where $\mathbf{\Lambda}_y=\mathrm{diag}(0,1,0)$ and $\mathbf{\Lambda}_z=\mathrm{diag}(0,0,1)$. Fig. 9 shows the distribution of chain choices in force control mode in the workspace based on LFNI before and after optimization.

4.2 Simulation of tracking errors in different control modes

In order to verify the effectiveness of the control mode de-

Algorithm 3. Simulate tracking errors in different control mode.

Input: $\boldsymbol{P}$: configurations in the trajectory
Output: $\boldsymbol{P}_e$: errors of the end effector along trajectory
1: set $i \leftarrow 0$, $N \leftarrow \text{size}(\boldsymbol{P})$
2: while $i < N$ do
3: $\boldsymbol{q} \leftarrow backward\_kinematics(\boldsymbol{P}(i))$
4: $\text{C} \leftarrow \{1, 2, 3, 4, \arg\min_{h=1,2,3,4} E(h), \arg\min_{h=1,2,3,4} EX(h), \arg\min_{h=1,2,3,4} EY(h), \arg\min_{h=1,2,3,4} EZ(h)\}$
5: for $k \leftarrow 0$ to 7 do
6: $\boldsymbol{q}_\tau(h) \leftarrow \boldsymbol{q}(h) + rand(-0.1mm, 0.1mm)$, $h \in \{1,2,3,4\}$ and $h \neq \text{C(k)}$
7: $\boldsymbol{p}_\tau \leftarrow forward\_kinematics(\boldsymbol{q}_\tau)$
8: $\boldsymbol{P}_e(i,k) \leftarrow \boldsymbol{P}(i) - \boldsymbol{p}_\tau$
9: $i \leftarrow i + 1$

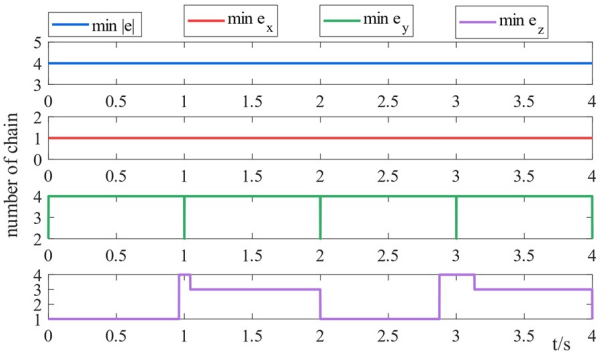

Fig. 10. Choice of chain in force control mode based on LFNI.

termination strategy, a tracking error simulation experiment is performed. The trajectory is the same as expressed in Eq. (33) and the algorithm is shown in Algorithm 3.

The simulation runs 100 times for manipulator B. The chosen chain in force control mode is shown in Fig. 10. And the average root mean square error along the trajectory is presented in Table 5, with units in μm.

It can be concluded that the TCP error along the X direction is smaller when chain 1 or chain 3 is selected to apply force control, and the TCP error along the Y direction is smaller when chain 2 or chain 4 is chosen to be in force control mode. These characteristics have a close relationship to the structure of the manipulator and match pretty well with the recommendation based on LFNI. Furthermore, according to Table 5, the performances based on LFNI all reach their goals if the position/force switching control is allowed.

5. Conclusions

This paper investigates the kinematic performance evaluation method based on the terminal error of a redundantly actuated parallel manipulator with 3 DOFs. The redundantly actuated parallel manipulator has many corresponding nonredundant counterparts. The terminal error of the one with the minimum terminal error among all the corresponding nonredundant manipulators is used to approximate the terminal error of the redundantly actuated manipulator. A local evaluation index, LFNI, is proposed to estimate the terminal error under the unit standard deviation of driving variables and the global index GFNI is defined by taking the worst case within the workspace. The GFNI is used in the optimum design of the RPU-UPR-2UPU manipulator, and the TCP errors of the manipulator along the *x*, *y*, and *z* directions are reduced after the optimum design. Furthermore, a control mode determination strategy based on LFNI is presented for the redundantly actuated parallel manipulator. This paper is useful for the performance evaluation and control mode determination of other redundantly actuated parallel manipulators with 3 DOFs. Future research will focus on the generalizability of the proposed method to more than 3 DOFs mechanisms.

Acknowledgments

This work is supported by the National Natural Science Foundation of China (Grant No. 52375502) and EU H2020 MSCA R&I Programme (no. 101022696).

References

[1] R. Lin et al., Type synthesis of 2R1T remote center of motion parallel mechanisms with a passive limb for minimally invasive surgical robot, *Mech. Mach. Theory*, 172 (2022) 104766.

[2] P. Lambert et al., Mobility of overconstrained parallel mechanisms with reconfigurable end-effectors, *Mech. Mach. Theory*, 171 (2022) 104722.

[3] X. Li et al., Optimal design of a kinematically redundant planar parallel mechanism based on error sensitivity and workspace, *J. Mech. Des.*, 145 (2022) 023305.

[4] X. Liang et al., Design, analysis, and optimization of a kinematically redundant parallel robot, *Actuators*, 12 (3) (2023) 120.

[5] K. Wen and C. Gosselin, Static model-based grasping force control of parallel grasping robots with partial cartesian force measurement, *IEEEASME Trans. Mechatron*, 27 (2) (2022) 999-1010.

[6] X. Liang et al., Kinematic analysis of three redundant parallel mechanisms for fracture reduction surgery, *Mech. Mach. Theory*, 188 (2023) 105400.

[7] Y. Li et al., A new method for type synthesis of 2R1T and 2T1R 3-DOF redundant actuated parallel mechanisms with closed loop units, *Chin. J. Mech. Eng.*, 33 (1) (2020) 78.

[8] D. Berendsen et al., A redundantly actuated 2-DOF 3RRR PKM with flexure joints: less is more, *Multibody Syst. Dyn.*, 59 (1) (2023) 1-17.

[9] R. Boudreau et al., Wrench capabilities of a kinematically redundant planar parallel manipulator, *Robotica*, 39 (9) (2021) 1601-1616.

[10] X. Luo et al., Kinematic calibration of the 3-degree-of-freedom redundantly actuated spatial parallel module of a five-axis hybrid machine, *Proc. Inst. Mech. Eng. Part B J. Eng. Manuf.*,

234 (9) (2020) 1185-1197.
[11] H. Wen et al., Dynamics and optimized torque distribution based force/position hybrid control of a 4-DOF redundantly actuated parallel robot with two point-contact constraints, *Int. J. CONTROL Autom. Syst.*, 17 (5) (2019) 1293-1303.
[12] H. Zhang et al., Force-position hybrid control of a novel parallel manipulator with redundant actuation, *2019 WRC Symposium on advanced Robotics and Automation (WRC SARA)*, Beijing, China (2019) 128-133.
[13] H. Zhang et al., Trajectory tracking control study of a new parallel mechanism with redundant actuation, *Int. J. Aerosp. Eng.*, 2020 (2020) e7178103.
[14] P. Yan et al., A 5-DOF redundantly actuated parallel mechanism for large tilting five-face machining, *Mech. Mach. Theory*, 172 (2022) 104785.
[15] J. Wu et al., Force optimization of planar 2-DOF parallel manipulators with actuation redundancy considering deformation, *Proc. Inst. Mech. Eng. PART C-J. Mech. Eng. Sci.*, 227 (C6) (2013) 1371-1377.
[16] J. Qiu et al., Torque optimization method of a 3-DOF redundant parallel manipulator based on actuator torque range, *J. Mech. Robot.*, 15 (2) (2023) 021005.
[17] X. Liu et al., Coordination dynamics and model-based neural network synchronous controls for redundantly full-actuated parallel manipulator, *Mech. Mach. Theory*, 160 (2021) 104284.
[18] C. Yang et al., Review of the performance optimization of parallel manipulators, *Mech. Mach. Theory*, 170 (2022) 104725.
[19] K. Chen et al., Topology design and performance optimization of six-limbs 5-DOF parallel machining robots, *Mech. Mach. Theory*, 185 (2023) 105333.
[20] G. Si et al., Integrating Dynamics into design and motion optimization of a 3-PRR planar parallel manipulator with discrete time transfer matrix method, *Math. Probl. Eng.*, 2020 (2020) e2761508.
[21] M. Díaz-Rodríguez et al., Performance index for dimensional synthesis of robots for specific tasks, *Robotics*, 11 (2) (2022) 51.
[22] J. P. Merlet, Jacobian, manipulability, condition number, and accuracy of parallel robots, *J. Mech. Des.*, 128 (1) (2005) 199-206.
[23] J. Wu et al., Dynamics and control of a planar 3-DOF parallel manipulator with actuation redundancy, *Mech. Mach. Theory*, 44 (4) (2009) 835-849.
[24] Y. Wang et al., Dynamics modeling, force optimization and force/position hybrid control for a Vex4 redundantly actuated parallel robot, *J. Mech. Eng.*, 58 (23) (2022) 65-74.
[25] H. Zhang et al., Trajectory tracking control study of a new parallel mechanism with redundant actuation, *Int. J. Aerosp. Eng.*, 2020 (2020) e7178103.

Yunfeng Jian received the B.S. degree in mechanical engineering from Tsinghua University, Beijing China, in 2022. He is currently working toward the Ph.D. degree in the Department of Mechanical Engineering, Tsinghua University, Beijing, China. His current research interests include machine tool error modeling, error measurement, and error compensation.

Jun Wu received the B.S. and M.S. degrees in mechanical engineering from Tianjin University, Tianjin, China, in 2000 and 2003, respectively, and the Ph.D. degree in mechanical engineering from Tsinghua University, Beijing, China, in 2008. He is currently a Professor in the Department of Mechanical Engineering, Tsinghua University. His current research interests include robot dynamics and control of parallel kinematic machine.